# Frequency modulated fiber optic electronic speckle pattern interferometry and its applications. Part II: Selected applications

ARTUR OLSZAK, KRZYSZTOF PATORSKI*

Warsaw University of Technology
Department of Mechatronics
Institute of Micromechanics and Photonics
Warsaw, Poland

*Electronic Speckle Pattern Interferometry (ESPI) is an important tool used in non-destructive testing, experimental mechanics and material property studies, medicine, etc. In the first part of this paper the system with extended measurement capabilities using fiber optics and frequency modulated semiconductor laser was presented. In this part representative applications of the system in experimental mechanics: long term measurements of out-of-plane displacements, vibration amplitude and phase analysis, in-plane displacement derivative measurements and contouring are described.*

## 1. Introduction

This second part of our paper describes selected applications of Electronic Speckle Pattern Interferometer with frequency modulated laser diode which was developed at our laboratory. The applications are devided into two parts confining statically and dynamically loaded (vibrating) objects to show the versatility of a fiber optics based system for laboratory as well as industry works.

## 2. Static measurements

### 2.1. Out-of-plane displacement measurements

One of the most frequent applications of ESPI systems is the measurement of out-of-plane displacements. Usually the decorrelation of speckle fields due to object rotations and translations can be kept reasonably small resulting in good modulation fringes. This feature is difficult to obtain in in-plane displacement arrangements. The phase shifting methods are also easy to realize by introducing a PZT device or by wavelength modulation of the laser source. Many interferometers for static out-of-plane displacement studies were reported in the literature. The first fiber optic systems were built by Davies [1] using "conventional" lasers. In 1990s semiconductor lasers have been applied in ESPI systems. Out-of-plane displacement sensitive interferometers for static displacement measurements differ from the arrangements for out-of-plane vibration measurements and contouring using the wavelength change only by the data evaluation software and possible laser diode wavelength modulation capabilities. Therefore, it is difficult to distinguish among them. Examples of such systems incorporating semiconductor lasers and based on optical fiber components are presented in [2, 3, 4, 5].

In this Section an example of application of out-of-plane sensitive ESPI configuration for investigations of long term stress relaxation in small components is presented. It is also an example of hybrid approach in solving problems in experimental mechanics.

* corresponding author: Krzysztof Patorski, Warsaw University of Technology, Department of Mechatronics, Institute of Micromechanics and Photonics, 8 Chodkiewicza Str. 02-525 Warsaw, Poland.

 

### 2.1.1. Hybrid methodology

The analyzes of today's designs are mainly done using the Finite Element Method (FEM). Often this is the only way to obtain results without the help of an experiment. The accuracy of computational solutions greatly relies on the agreement of model assumptions including real load levels and constraints put on the component under design. Determination of material properties such as Young's modulus, or relaxation constant, is essential for obtaining accurate results. They can be found in the literature usually as approximate values for particular material types. Often, however, it is required to conduct an experiment to obtain exact values of material constants.

These problems can be successfully solved by the combination of non-invasive optical methods with the FEM modeling to form a hybrid solution system. Speckle interferometry can supply information for quantitative calculation of material properties. Fringe images acquired during the test runs give the location of stress concentrations and can indicate areas where the modeling mesh must be denser. Values of stresses and displacements rendered from the optical setup can be used to specify boundary conditions, to update material data banks, or to supply designers with data where they are not available.

### 2.1.2. Relaxation process

The stress relaxation process relates to the decrease of stress due to rearrangements in the material. A typical stress relaxation curve is shown in Fig. 1.

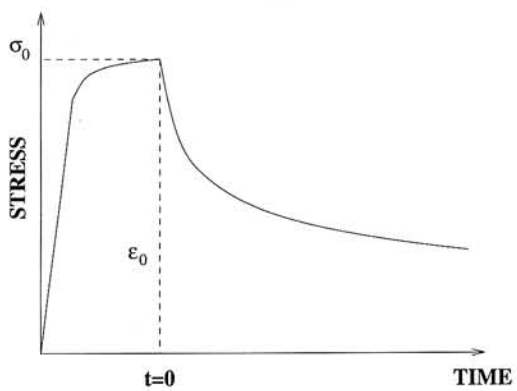


Fig. 1. A typical stress relaxation curve.

Following application of the load ($t = 0$) the internal structure of the material changes resulting in a decrease of stress while the strain is held constant. The time dependent stress behavior can be approximated by a logarithmic curve. Determination of the time rate of stress changes is important for predicting long term behavior of the material. Usually the time of the full relaxation of the stress is of the order of hundreds of hours and depends on the environmental conditions, mostly the temperature. ESPI can be used to monitor the changes of the shape of the sample and the results obtained in this way can be used to determine the shape of the long term stress relaxation curve.

### 2.1.3. Experimental procedure

The arrangement used in the experiment was an out-of-plane sensitive configuration ESPI presented in Fig. 3 of Part I of this paper. In this particular experiment the phase shifting was realized by a PZT drum with a wrapped fiber, controlled directly from the computer by means of a data acquisition board. Images grabbed during the experiment were transferred to the host computer memory for the computation of the phase map and stored in a specialized data base. Then, based on the phase maps, displacements were determined and transferred to FEM software in order to compute stress changes in the specimen due to the relaxation process.

There is no theoretical formulation for the quantitative analysis of the relaxation problem. Therefore modeling must be based on the experimental data. The out-of-plane arrangement described in Part I of this paper was used to determine time-dependent behavior of a cantilever beam made of brass. Determination of the stress relaxation of materials which are used to manufacture microelectronic connectors is essential for the design of reliable electrical interconnections. The test sample was rigidly fixed at the lower end and loaded with a constant displacement in the $z$ direction applied at the upper end. The displacement was calculated so that the maximum stress induced in the beam was approximately 10% of the yield point of the material. The cantilever beam was illuminated by a parallel beam of laser light normal to the surface to ensure the sensitivity of the system only in the out-of-plane direction. The load was applied at time $t = 0$. Immediately after loading of the sample, the reference image was taken and stored in the computer. Consecutive series of images were taken at specific time intervals in order to calculate time-dependent deformation of the cantilever beam due to the relaxation process.

### 2.1.4. The FEM model

For the FEM modeling of the displacements and stresses of the beam, a commercial software package

COSMOS/M was used. The stresses induced in the beam were in the elastic response range of the material, so a linear static analysis was used. The beam was modeled by means of solid linear 8-nodded elements. A brass cantilever beam of dimensions 20 *mm* × 1.25 *mm* × 0.25 *mm* was used. The modulus of elasticity of the material used for the test samples was 110 *GPa*. In the model developed the boundary conditions at the bottom of the beam were represented by setting all six degrees of freedom to zero. The beam was loaded at the free end with a known displacement in the $z$ direction. Representative results of the modeling are shown in Fig 2.

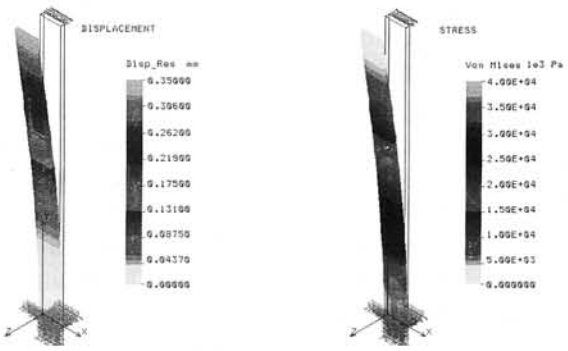


(a) (b)

Fig. 2. FEM determined displacements and stresses in the cantilever beam test sample subjected to pure bending.

For the data evaluation the phase map obtained by the phase stepping method from ESPI must be transferred to the FEM package. Since the coordinates of the nodes usually do not coincide with coordinates of locations of pixels on the object, an interpolated displacement value must be calculated. In the software used in this study a bilinear interpolation scheme was employed to obtain the data between the pixels. The geometry transformation from the screen coordinates of the ESPI system into the FEM domain was calculated using the markers painted on the object surface. The file with results from ESPI, converted into the proper format, was transferred to the FEM package to correct the values of displacements obtained from modeling and to recalculate stresses inside the sample.

## 2.1.5. Results

A series of experiments was conducted in order to obtain the time dependent characteristics of the relaxation process of the test samples. These samples were observed over the period of 120 hours. Series of speckle interferograms were taken at the specific time

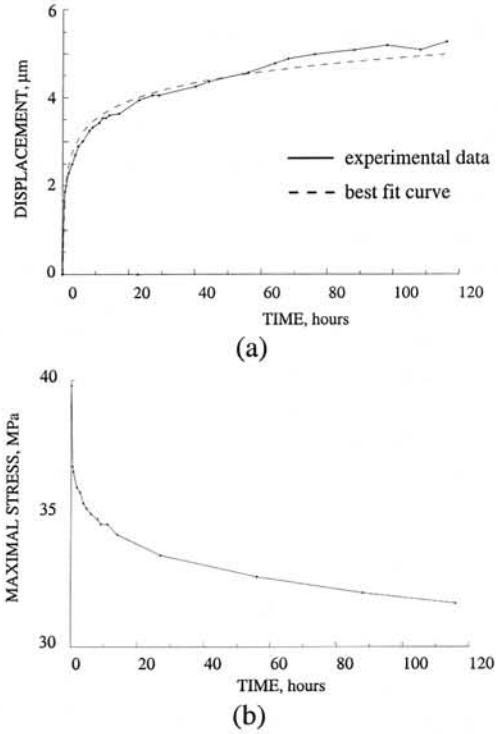


Fig. 3. a) Maximum displacement of the test sample during the relaxation process; b) Maximum of stress in the cantilever beam FEM model based on the interferometric data.

intervals. The time between acquisition of images varied from 15 *min* after the samples loading up to 4 hours at the end of the observation period.

In the case of a cantilever beam its maximum deformation from the "original" shape before applying the load was assumed as a descriptive parameter of the relaxation process. The time plot of displacement with fitted exponential curve is shown in Fig. 3a.

Coefficients of the fitted curve can be used for modeling of time dependent phenomena by the FEM software. The highest time rate change of displacement due to stress relaxation was observed immediately following application of the load. The rate decreased monotonically until 20 hours after the loading. Then, the rate changed nearly linearly at approximately $13\frac{nm}{hour}$ for the rest of the test sequence.

Based on the data obtained from the ESPI system, stress distribution in the FEM model of the test sample was recalculated. The time plot of the maximum stress induced in the cantilever beam is shown in Fig. 3b. The interferometric data were used to update the displacements of the cantilever beam model using the method described in Section 2.1.4 and the stress distribution was then recalculated. According to Fig. 3a, the change in displacement due to stress relaxation was 5% of the displacement applied to the beam at the instant of the

 

loading. This change in the displacement has led to 10% stress decrease as compared with the initial stress level at the instant of loading, Fig. 3b, during 120 hours long test sequence.

The accuracy of measurements was mainly determined by the phase step error and the camera noise. The phase step calibration was done with the accuracy of fringe/20 which corresponds to 20 nm. The camera noise was estimated to be the least significant bit and was about 1.5% for the modulation of 128 gray levels. The total error of measurements was smaller than 5%. Although the calculated changes are of the order of estimated error for the FEM method, a well behaved time characteristic was observed.

## 2.2. Displacement derivative measurements

Speckle pattern shearing interferometry (ESPSI) is an optical method for determining the derivatives or their approximate values of surface displacements. It was developed independently by Leendertz and Butters [6] and Hung and Taylor [7]. The principle is to interfere two mutually laterally displaced images of the same object. When two speckle patterns corresponding to two different object states (for example, before and after applying the load) are compared by subtraction, the correlation fringes connecting the points of equal displacement gradients are formed. The direction of displacement (shear) between the two speckle patterns determines the direction of the partial derivative averaged over the shear distance. In practice rather large shear values in comparison with smallest object deformations are used to increase the sensitivity of the method. Hence it is difficult to talk about generating the displacement derivatives required for strain measurements. However, the application in non-destructive testing is very promising.

The advantages of ESPSI over the conventional ESPI using a reference beam are the reduced susceptibility to vibrations and the compensation of tilts in the shear direction. Nevertheless, rigid body motions and rotations must be under control to avoid decorrelation effects [8]. The ESPSI method has found main application in non-destructive testing of industrial products and materials, rather than in strain measurements. The reason is that strain concentrations are mapped as local disturbances in fringe patterns, which can be readily detected and used for global object assessment. This fact might be the reason that almost all studies presented up to now have concerned the detection of out-of-plane displacements.

### 2.2.1. Digital in-plane electronic speckle pattern shearing interferometry – principle

Below, as an example, we describe a novel implementation of the ESPSI working in the in-plane displacement configuration to produce maps of in-plane and out-of-plane displacement derivatives. The principle of the method [9, 10, 11] is to individually shear the two wavefronts that would otherwise produce a conventional in-plane displacement electronic speckle interferogram/correlogram. In this way two lateral shear interferograms are sequentially produced and recorded. The phases are calculated and their subtraction or addition is performed by software to yield the derivatives of in-plane and out-of-plane displacements, respectively.

At this moment it is worthy to mention another recently proposed approach to determine the partial derivative of out-of-plane displacement in the modified in-plane ESPI configuration [12]. The information required is again obtained by software subtraction of phase functions calculated, this time, from different two primary interferograms: a conventional in-plane displacement interferogram and one with object speckle fields laterally displaced in the image plane. Very good coincidence between the theoretical and experimental results has been obtained. Two channel configuration enables simultaneous recording of the component speckle fields.

### 2.2.2. Experimental work

The principle [9, 10 11] can be implemented in an optical path imbalanced Michelson interferometer, used as a shearing device in front of the CCD camera, see Figs. 7 and 8 of Part I. The automatic fringe pattern analysis for retrieving the phases uses the temporal phase stepping approach realized by tuning the light

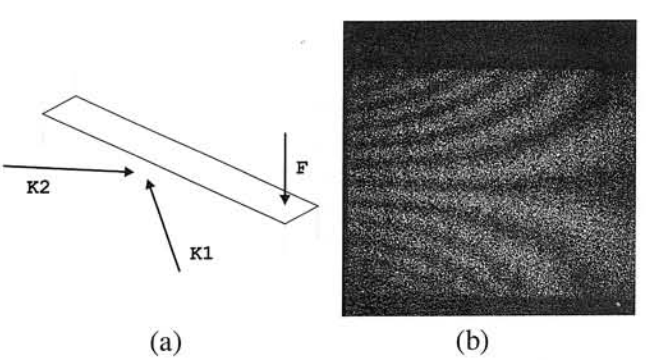


Fig. 4. a) Schematic of loading of the cantilever beam used in the experiment. F, the loading force, $\vec{K_1}$ and $\vec{K_2}$ ilumination directions. The shear applied was in $K_1 - K_2$ plane. b) In-plane displacement fringes obtained in setup a).

wavelength of the laser diode [13]. In this way mechanical adjustments and nonlinearities of interferometer elements are avoided.

In the setup the angle of incidence of beams was 45°, the shear $\Delta x$ in the object plane was set to 2.5 mm and the used wavelength was 782 nm (laser diode Hitachi 7851G), yielding the distance between the displacement fringes equal to $\frac{\lambda}{2\sin\Theta} = 535\,nm$, and for the derivative fringes equal to $\frac{\lambda}{2\Delta x\sin\Theta} = 2.2 \cdot 10^{-2}\%$. During the measurements the object with the interferometer was placed on the antivibrational table and insulated in a styrofoam chamber from the environment to avoid the influence of air convection. The data acquisition time (grabbing images and transferring to the host computer) was about 6s. Due to little output light available the summarized measurement error was limited by the camera noise and decorrelation of speckle fields. Object under investigation was a cantilever beam, 25 mm high, 25 mm thick and 150 mm long, made of a stiff epoxy polymer loaded with a force perpendicular to the shear and the observation directions, Fig. 4. Another investigated object was a disk in compression with a hole and horizontal cut, Fig. 5.

The measurements were done with the accuracy of about fringe/20 which corresponds to strain value of $0.1 \cdot 10^{-2}\%$. After unwrapping the phase maps were treated twice with averaging filter $9 \times 9$ pixels to remove the spike noise from remaining bad pixels. For smoothly varying phase maps, as in the experiments, this was not a limiting factor. However, in some cases the size of the averaging window should be reduced to avoid the decrease of accuracy.

## 2.3. Contouring

Remote shape measurement is one of the most important issues in modern experimental mechanics. Hybrid methodology is making its way to industrial and research laboratories and integration of various specialized design packages. For example, rapid prototyping, FEM, FBM, CAM/CAD, require precise information about the 3-dimensional shape of the object.

The ESPI contouring method by wavelength modulation originated from holographic interferometry and was demonstrated to work successfully with ESPI systems [14]. However, its use was limited because of the lack of easily tunable laser source. Commercial availability of tunable semiconductor lasers sources changed the situation and ESPI systems were

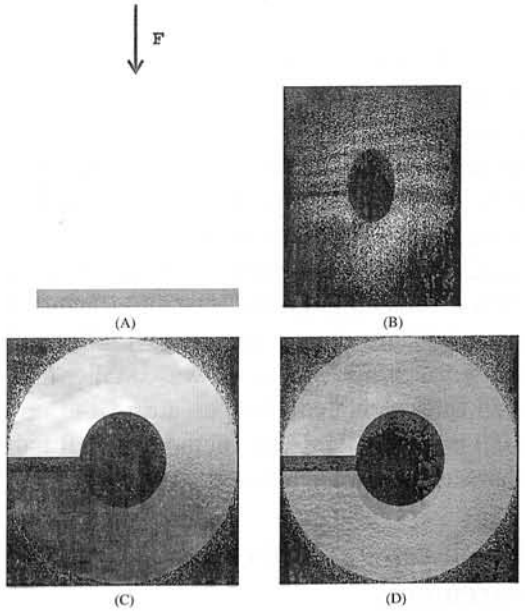


Fig. 5. Measurement results for a cut disk in compression. A) loading schematics, B) illustrative derivative fringes (interval $2.2 \cdot 10^{-2}\%$), C) the in-plane derivative obtained by subtraction of phase maps from two channels, and D) the out-of-plane derivative, respectively.

applied to contouring using the wavelength change, as well. Two-wavelength contouring was introduced in holographic interferometry [15] but soon reports on ESPI systems based on using this approach were reported [16]. Atcha [17] and Huang [5] reported all fiber systems based on a laser diode working in contouring mode for measurements of the surface profile and slope, respectively. In this Section the system presented in Part I will be demonstrated to work as a contouring device. The results of measurements of test objects will be presented.

### 2.3.1. The experimental setup and procedure

The interferometer employed for the experiments was configured as for the out-of-plane displacement measurements (see Fig. 3 of Part I). The illumination direction was coincident with the observation direction in order to maximize the system sensitivity. The four-step phase shifting method was employed for measurements. A reference frame of an object under test was acquired prior the wavelength change and stored in the frame grabber operational memory. The wavelength emitted by the laser can be changed by altering the temperature of the junction or the driving current. The frames coming from the CCD camera were subtracted in real time from the reference frame and displayed on the system monitor. In order to achieve the best results the adjustments of the system sensitivity could be

 

made in real time by continuous observation of the amount of the wavelength change.

After setting the contour interval, four phase shifted frames were acquired and sent to the host PC for further processing. The phase shift was realized by the current induced wavelength modulation or using a PZT phase shifter introduced in the reference beam. If the current modulation is used for phase shifting the intensity of acquired images changes introducing errors in the retrieved phase [18]. Normalization of the image intensity must be used or the six-step phase shifting algorithm proposed by Ishii [19] must be applied to avoid this influence. Another problem arises from the fact that during the wavelength induced phase shift the difference in registering wavelengths between the reference and measurement images changes during the phase shifting process. It causes differences in contour interval values between the acquired frames. In this case an additional phase step resulting from the phase shift must be taken into account. It can be compensated for using the standard Carré algorithm providing the intensity images are normalized. In measurements with the PZT phase shifter the standard four-frame, $\frac{\pi}{2}$ phase shift algorithm was used to extract the phase. To ensure that contour surfaces were plane the object was illuminated by plane wavefront produced by a collimating lens.

### 2.3.2. Experimental results

As the test objects a corner of a cube and a roof with $\frac{\pi}{2}$ angle were chosen. A series of measurements was conducted with the described setup for different changes of the junction temperature ranging from 0.1°C to 2.0°C. For the time of measurements the object and the interferometer were placed on a vibration isolating table in an insulating chamber made of styrofoam. Both objects were covered with a thin layer of titanium dioxide for better light reflectivity.

The temperature-wavelength and current-wavelength coefficients determined for the laser diode used in the measurements were $0.092 \pm 0.003 \frac{nm}{^{\circ}C}$ and $0.0068 \pm 0.0005 \frac{nm}{mA}$, respectively. However, it should be noted that for both phenomena the wavelength characteristics can be regarded as linear only for the parts between the mode hops. Identification of the current and temperature values for which the mode hops occur can be done using a high resolution spectrometer. For the diode used in the setup there were no mode hops observed in the range of used current and temperature. The method of interferometer calibration described in [20] can be also used to assess both the wavelength-current coefficient and to localize the mode hops on the laser characteristics.

The non-planar illumination errors are removed by subtracting the phase measured for a plane perpendicular to the observation direction, placed at the distance equal to the distance to the object.

A set of test measurements for different wavelength changes was performed. Representative measurements results are shown in Figs. 6 through 9.

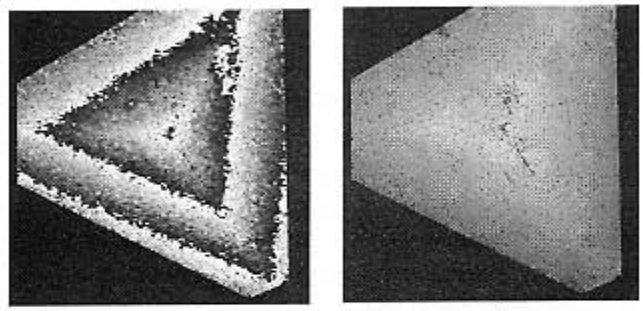

(a) (b)

Fig. 6. Representative results of remote contouring by wavelength change: corner cube measurements. a) wrapped phase showing contours, b) unwrapped phase. The fringe interval is 12 mm, it corresponds to the temperature change of 0.55°C.

The observed range of contour interval was several millimeters to 0.7 mm and depended on the magnitude of the temperature changes. In Fig. 6 the extracted phase map (wrapped and unwrapped) for a cube, isometric view, is shown. Contour interval was 12 mm (the temperature change was 0.55°C) which corresponds to the wavelength change of 0.03 nm. In Fig. 7 a 3-D-plot of the recovered shape is presented. Similar results for a roof are shown in Figs. 8 through 9. In this case the contouring interval was 5.6 mm corresponding to the junction temperature change of 1.19°C and the wavelength change of 0.11 nm. Figure 8 shows the wrapped and unwrapped phase images and Fig. 9 shows a 3-D view of the recovered shape.

The achieved contouring sensitivity was ranging from several millimeters to 0.7 mm. Temperature changes of the laser junction by 0.1° through 8.5°C produced wavelength changes of the laser light of up to 0.8 nm. Observed correlograms had good contrast which slightly decreased with the increase of the wavelength difference. The correlation fringes can be observed in real time on the monitor screen and allow continuous adjustments of the fringe interval. For current induced phase

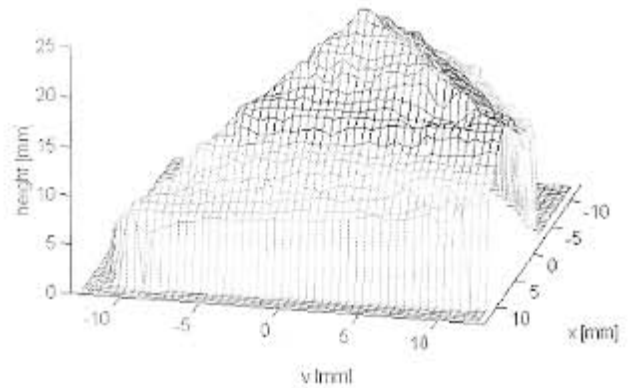


Fig. 7. Representative results of remote contouring by wavelength change: 3D plot of the shape of the corner cube under test.

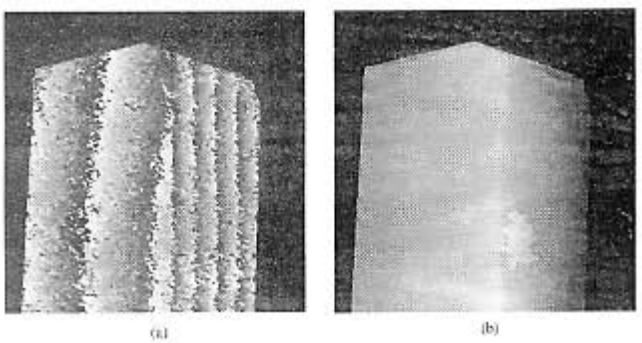


Fig. 8. Representative results of remote contouring by wavelength change: straight edge measurements. a) wrapped phase showing contours, b) unwrapped phase. The fringe interval is 5.6 mm and corresponds to the temperature change of 1.19°C. A phase unwrapper failure is visible.

shifting the error compensating algorithm must be used. Both processes are fully automated. The phase shift was calibrated with the accuracy of fringe/20. The modulation of correlation images was optimized by adjusting the intensity ratio of the reference to the object beams.

## 3. Dynamic measurements

### 3.1. Vibration amplitude measurements by the time average method

Heterodyning is a widely used interferometric technique for recovering the amplitude of a vibrating object. In "conventional" ESPI arrangements the sinusoidal modulation of the optical phase in the reference beam is introduced by vibrating mirrors on PZT transducers [21, 22, 23]. In fiber optic systems, the fiber wrapped PZT transducers were reported in [3, 24]. Atcha and Tatam in [25] have presented a setup employing the wavelength modulation of a semiconductor laser to introduce a sinusoidal signal in the

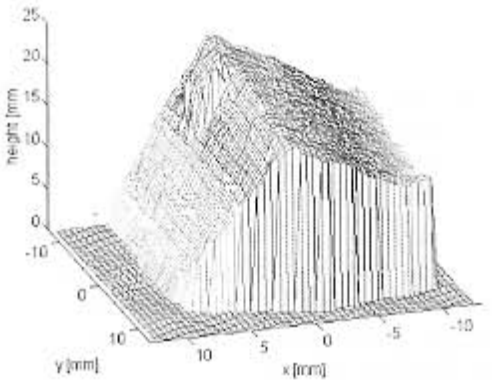


Fig. 9. Representative results of remote contouring by wavelength change: 3D plot of a roof.

reference beam. The visualization of vibrations was achieved by subtraction of consecutive TV frames. In this method $\pi$ shift between the frames was introduced by a standard PZT phase shifting device.

In this Section the attention is focused on the ESPI system in which modulation of the laser diode emission is used for simultaneous realization of the heterodyning process and phase shifting by $\pi$ between consecutive frames for visualization of high contrast vibration fringes.

The fiber optics ESPI system using a semiconductor laser was configured for out-of-plane displacement investigations as described in Part I (Fig. 3). In the time-average method the intensity pattern resulting from the interference between the beam reflected from the vibrating object and the reference beam is integrated within duration of one TV frame and registered by a CCD camera.

For the experiment an aluminum plate was chosen with dimensions of $100 \times 65 \times 1$[mm]. The plate was rigidly fixed at one of the shorter edges and excited by a piezoceramic transducer mounted at the back side. The object was painted white for better reflectivity. Sinusoidal variable phase generator was used to generate heterodyning signal and drive the PZT attached to the test object. First the resonant frequencies of the aluminum plate were found by scanning from 0 to 1.3 kHz. There are three first resonant frequencies in this range corresponding to the first and second bending and torsion modes. At these frequencies the measurements of vibration amplitude were done.

The locus of the 0-th order fringe was adjusted by changing the amplitude and phase of the reference signal. The $\pi$ signal amplitude was found by observing the maximum intensity of the object image at rest. It corresponded to the changes of laser diode current of 0.7mA. For the purpose of this experiment the influence of intensity changes caused by laser driving current

 

changes was neglected. However, it can be compensated by normalizing the image intensity using the PIN readout of the laser. For each measurement a set of three images with mutual phase shift of $\frac{\pi}{2}$ was acquired and phase maps were calculated using image processing system developed at Optical Engineering Division.

The accuracy of the phase shift was fringe/20. The total accuracy of the measurements was limited by the noise of the CCD camera and amounted to 5% due to the low modulation of correlation images. To suppress the spike noise and smooth the results the phase images were treated twice with $5 \times 5$ averaging filter.

## 3.2. Small vibration amplitude and phase measurements

The state of a harmonically vibrating object is described by the vibration amplitude and phase distributions. The technique employed in this Section is applied to measurements of small amplitude vibrations up to about 40 nm, which is often sufficient to analyze the behavior of the object. The method presented in this Section was first introduced by Høgmoen and Lǿkberg [26] and extended by others [27, 28, 29]. The literature reports successful applications for measurements of loudspeaker behavior, human ear drum, mechanical components, etc. For the measurements of amplitude and phase of high amplitude vibrations the stroboscopic method can be used [30].

The interferometer was configured for out-of-plane displacement measurements as described in Part I (Fig. 3). Two consecutive images of the vibrating object were shifted by $\pi$ and subtracted using image processing board placed in the host computer following the same methodology as for the heterodyning method. As an object a circular membrane rigidly fixed along the edge was chosen. A PZT transducer mounted on the rear side of the membrane was used to excite its lowest fundamental vibrational modes. The membrane was made of a low carbon steel and was 135 mm in diameter and 0.33 mm thick. The front surface was covered with a thin layer of titanium dioxide for better reflectivity. No influence of this layer on the vibrational patterns was observed. During the experiments the amplitude and phase of the fundamental modes of the membrane were investigated over the range 0 to 1300 Hz.

For each measurement a set of four images, phase shifted by $\frac{\pi}{2}$, were acquired. Additionally two images were grabbed before the measurement cycle for the factor calibration.

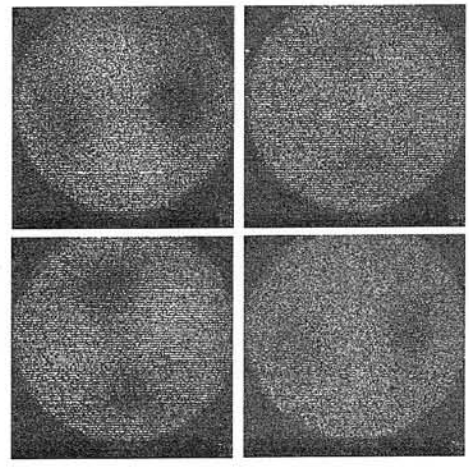

Fig. 10. Vibrational patterns of a membrane rigidly fixed along the circumference for fundamental frequency of 563 Hz.

The finite element modal analysis for the object under investigation was done using FEM package COSMOS/M. The object was modeled and analyzed using linear model with thin 3-node shell elements. Results obtained this way were compared with the observed patterns to confirm the validity of the experimental technique.

Representative results are shown in Figs. 10 through 13. In Fig. 10 the phase shifted vibrational patterns are presented, corresponding to the fundamental mode at the frequency of 563 Hz. The extracted amplitude and phase for the same mode are shown in Fig. 11. Figure 12 shows the theoretical results corresponding to the case of Fig. 10 and 11. The resonant frequency calculated from the FEM analysis was 593 Hz.

The results shown in Fig. 13 were obtained for the same object but at the frequency of 1260 Hz. Figure 14 shows the theoretical predictions of the vibrational pattern for the same mode obtained by the FEM calculus. The obtained resonant frequency was 1490 Hz. The difference is caused by the mass of the PZT transducer attached to the back side of the membrane. Its in-

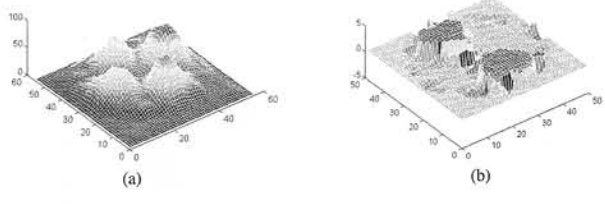


Fig. 11. Amplitude (a) and phase (b) recovered from data shown in Fig. 10.

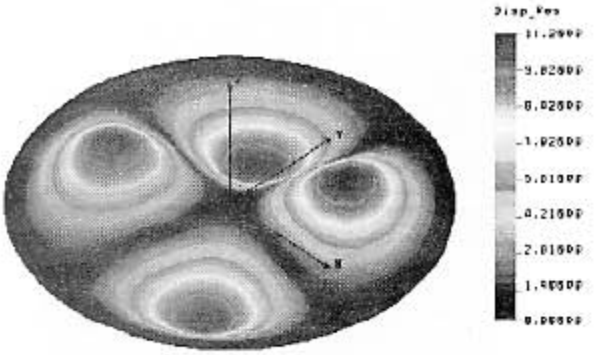

Fig. 12. Theoretical results corresponding to the fundamental mode, shown in Fig. 10, at 593 Hz.

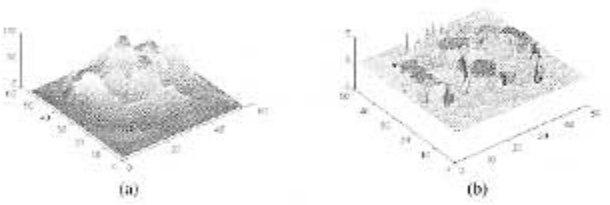


Fig. 13. Amplitude (a) and phase (b) of a membrane rigidly fixed along the circumference for the fundamental mode at 1260 Hz.

fluence is also visible as the asymmetricity of the vibrational patterns.

The vibration phase discontinuities visible on the plots are caused by the phase unwrapping strategy. The phase can assume two values: 0 and $\pi$. While zero is unwrapped properly the $\pi$ value is a threshold for adding or subtracting the $2\pi$ jump. The image noise

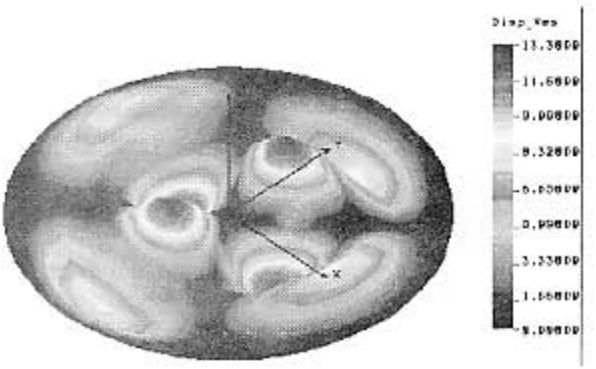

Fig. 14. Theoretical results corresponding to the fundamental mode shown in Fig. 13 at 1490 Hz.

makes the unwrapper to subtract in certain points and the plots occur noisy while the phase oscillates around the correct the value of $\pi$.

The accuracy of measurements was limited by the electronic noise of the camera due to low light level in the object plane. The accuracy was estimated to be 1.5%. This value corresponds to about 5 nm in displacement amplitude. However, the frame averaging lowered this error to fringe/20, i.e., to about 2.5 nm. Phase shifting was done with an accuracy of 2.5° which can be neglected in the total accuracy considerations. Prior to the calculations the intensity images were filtered twice with a $5 \times 5$ averaging filter. The total error of the amplitude and phase measurements was about 10%.

## 4. Conclusions

In this paper we presented a number of applications of an improved fiber optic ESPI system using diode laser. They range from static analysis of displacements to measurement of amplitude and phase of vibrations under dynamic load. The system advantages are portability and small dimensions, powerful software and lack of adjustable mechanical parts used for measurement purposes. Achieved accuracy is comparable to other commercially available devices of this kind with simultaneously extended range of applications. The selected examples show a potential of presented interferometer system as a viable alternative to conventional techniques used in laboratory and industrial experimental mechanics such as speckle photography, photoelasticity or strain gauges.

## 5. Acknowledgements

This work was financially supported by the State Committee of Scientific Research Grant No. 7TO7D 011 08.

## References

1. J.C. Davies, C.H. Buckberry, J.D.C. Jones and C.N. Panell: *Development and application of a fibre optic electronic speckle pattern interferometer* (ESPI)., Proc. SPIE **863**, (1987) 194.
2. R. Jones and C. Wykes, *Holographic and Speckle Interferometry*: Cambridge University Press (1989).
3. J. D. Valera, D. Harvey and J.D.C. Jones: *Automatic heterodyning in fiber optic speckle pattern interferometry using laser velocimetry*., Opt. Eng. **31**, (1992) 1646.
4. H. Atcha and R.P. Tatam: *The use of laser diodes*

 

*and monomode optical fibre in electronic speckle pattern interferometry.*, Proc. SPIE **1584** (1991) 221.

5. J.-R. Huang: *Optoelectronic Speckle Shearing Interferometry.*, Ph.D. thesis, Cranfield University, UK (1996).
6. J.A. Leendertz and J.N. Butters: *An image-shearing speckle pattern interferometer for measuring bending moments.*, J. Physics E, **6**, (1973) 1107.
7. Y.Y. Hung and C.E. Taylor; Speckle-shearing interferometric camera – a tool for measurement of derivatives of surface displacements., Proc. SPIE **41**, (1973) 169.
8. M. Owner-Petersen: *Digital speckle pattern shearing interferometry: limitations and prospects.*, Appl. Opt., **30**, (1991) 2730.
9. K. Patorski and A. Olszak: *Modified in-plane electronic speckle pattern shearing interferometry.*, Opt. Eng., **36**, (1997) 2010.
10. W. Steichen, L.X. Yang and Schuth: *TV-shearography for measuring of 3d-strains.*, Strain, **32**, (1996) 49.
11. P.K. Rastogi: *Measurement of in-plane strains using electronic speckle and electronic-shearing pattern interferometry.*, J. Mod. Opt., **43**, (1996) 1577.
12. K. Patorski and A. Olszak: *Opto-digital determination of the derivative of out-of-plane displacement using modified in-plane* (ESPI)., Proc. Fringe'97 (1997), in press.
13. K. Patorski and A. Olszak: Modified in-plane electronic speckle pattern shearing interferometry (ESPSI)., Proc. SPIE **2860**, (1996) 256.
14. G. Gulker, O. Haack and K.D. Hinsch: Two-wavelength electronic speckle pattern interferometry for the analysis of discontinuous deformation fields., Appl. Opt., **31** (1992) 4519.
15. R.P. Tatam, J.C. Davies, C.H. Buckberry and J.D.C. Jones: *Holographic surface contouring using wavelength modulation of laser diodes.*, Opt. Laser Technol., **22**, (1990) 317.
16. A.F. Fercher, U.Vry and W.Wermer: *Two wavelength speckle interferometry on rough surfaces using mode hopping diode laser.*, Opt. Lasers Eng., **11**, (1989) 271.
17. H. Atcha, R.P. Tatam, J.C. Davies, C.H. Buckberry and J.D.C. Jones: *Surface contouring using TV holography.*, Proc. SPIE, **1504**, (1991) 221.
18. P. Hariharan: *Phase-stepping interferometry with laser diodes. 2: Effects of laser wavelength modulating.*, Appl. Opt., **28**, (1989) 1749.
19. Y. Ishii and R. Onodera: *Laser-diode phase shifting interferometer insensitive to the changes in the laser power.*, Proc. SPIE , **2544**, (1995) 173.
20. A. Olszak and R.P. Tatam: *Calibration of optical path imbalance in fibre optic ESPI system.*, Meas. Sci. Technol., in press (1997).
21. O.J. Løkberg and K. Hogmœn: U*se of modulated reference wave in electronic speckle pattern interferometry.*, J. Phys. E., **9**, (1976) 847.
22. R.J. Pryputniewicz and K.A. Stetson: Measurement of vibration patterns using electo-optic holography., Proc. SPIE, **1162**, (1989) 456.
23. K. A. Stetson, W.R. Brohinsky, J. Wahid and T. Bushman: *An electro-optic holography system with real-time image processing.*, J. Nondestruct. Eval., **8**, (1989) 69.
24. J.D. Valera, A.F. Doval and J.D.C. Jones: *Combined fibre optic laser velocimeter and electronic speckle pattern interferometer with a common reference beam.*, Meas. Sci. Technol., **4**, (1993) 578.
25. H. Atcha and R.P. Tatam: *Heterodyning of fibre optic electronic speckle pattern interferometers using laser diode wavelength modulation.*, Meas. Sci. Technol., **5**, (1994) 704.
26. K. Høgmoen} and O.J. Løkberg: *Detection and measurement of small vibrations using electronic speckle pattern interferometry.*, Appl. Opt., **16**, (1977) 1869.
27. S. Ellingsrud and O.J. Løkberg: *Full field amplitude and phase measurement of loudspeakers by using TV-holography and digital image processing.*, J. Sound Vibr., **168**, (1993) 193.
28. S. Ellingsrud and G.O. Rosvold: *Analysis of a data-based TV-holography system used to measure small vibration amplitudes.*, J. Opt. Soc. Amer. A, **9**, (1992) 237.
29. O.J. Løkberg, R. Rustad and M. Espeland: *Reconstruction of sound fields using TV-holography.*, Proc. SPIE, **2358**, (1994) 305.
30. D.J. Anderson, J.D. Valera and J.D.C. Jones: *Electronic speckle pattern interferometry using diode laser stroboscopic illumination.*, Meas. Sci. Technol., **4**, (1993) 982.